AD-A172 612 USE OF INCOHERENCE TO PRODUCE SMOOTH AND CONTROLLABLE 1/1
IRRADIATION PROFILE (U) NAVAL RESEARCH LAB WASHINTTON
DC R H LEHMBERG ET AL 14 AUG 86 NRL-MR-5829
UNCLASSIFIED DE-AI08-79DP40092 F/G 20/5 NL

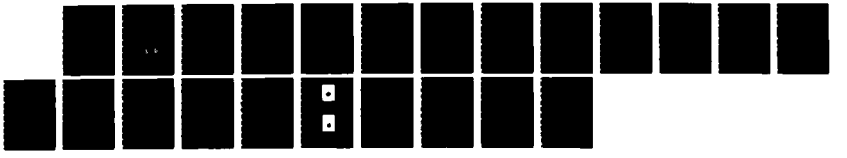

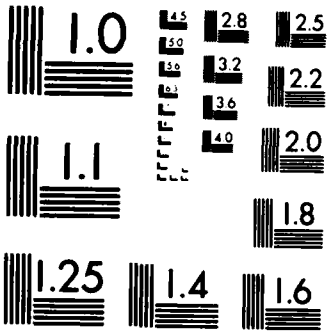

Naval Research Laboratory

Washington, DC 20375-5000 NRL Memorandum Report 5829 August 14, 1986

Use of Incoherence to Produce Smooth and Controllable Irradiation Profiles with KrF Fusion Lasers

R. H. LEHMBERG

Laser Plasma Branch
Plasma Physics Division

J. GOLDHAR

University of Maryland
College Park, MD 20740

Approved for public release; distribution unlimited.

SECURITY CLASSIFICATION OF THIS PAGE

REPORT DOCUMENTATION PAGE

1a REPORT SECURITY CLASSIFICATION UNCLASSIFIED	1b RESTRICTIVE MARKINGS None
2a SECURITY CLASSIFICATION AUTHORITY	3 DISTRIBUTION / AVAILABILITY OF REPORT Approved for public release, distribution unlimited.
2b DECLASSIFICATION / DOWNGRADING SCHEDULE	
4 PERFORMING ORGANIZATION REPORT NUMBER(S) NRL Memorandum Report 5829	5 MONITORING ORGANIZATION REPORT NUMBER(S)
6a NAME OF PERFORMING ORGANIZATION Plasma Physics Division 6b OFFICE SYMBOL (If applicable) Code 4730	7a NAME OF MONITORING ORGANIZATION Laser Plasma Branch
6c ADDRESS (City, State, and ZIP Code) Naval Research Laboratory	7b ADDRESS (City, State, and ZIP Code) 4555 Overlook Avenue, SW Washington, DC 20375-5000
8a NAME OF FUNDING / SPONSORING ORGANIZATION Department of Energy 8b OFFICE SYMBOL (If applicable) DP-23	9 PROCUREMENT INSTRUMENT IDENTIFICATION NUMBER DE-AI08-79DP40092
8c ADDRESS (City, State, and ZIP Code) U.S. Department of Energy Office of Inertial Fusion (DP-23) Washington, DC 20545	10 SOURCE OF FUNDING NUMBERS PROGRAM ELEMENT NO: DOE PROJECT NO: 47-0859-0- TASK NO: AI08-79DP40092 WORK UNIT ACCESSION NO.
11 TITLE (Include Security Classification) Use of Incoherence to Produce Smooth and Controllable Irradiation Profiles with KrF Fusion Lasers	
12 PERSONAL AUTHOR(S) Lehmberg, R.H. and Goldhar, J.	
13a TYPE OF REPORT Memorandum 13b TIME COVERED FROM _____ TO _____	14 DATE OF REPORT (Year, Month, Day) 1986 August 14 15 PAGE COUNT 22
16 SUPPLEMENTARY NOTATION	
17 COSATI CODES FIELD / GROUP / SUB-GROUP	18 SUBJECT TERMS (Continue on reverse if necessary and identify by block number)

19 ABSTRACT (Continue on reverse if necessary and identify by block number)

A technique called Echelon-Free Induced Spatial Incoherence, is proposed for producing smooth, controllable target beam profiles with large KrF fusion lasers. The idea is basically an image projection technique that projects the desired time-averaged spatial profile $F(\vec{x})$ onto the target via the laser system, using partially-coherent broadband light. The information needed to reproduce $F(\vec{x})$ is transported through the system by a multitude of independent coherence zones, whose diameters are small in comparison to scale lengths of linear aberration and gain nonuniformities; as a result, $F(\vec{x})$ remains relatively insensitive to these effects. This concept is closely related to the Induced Spatial Incoherence (ISI) technique used with glass lasers, except that it does not require echelons at the output of the system. An analysis is carried out to evaluate the perturbations of $F(\vec{x})$ due to linear aberration, self-focusing, gain saturation, and diffraction. It shows that under conditions applicable to large KrF lasers, the perturbations will result in a small broadening and smoothing of $F(\vec{x})$, whose functional form should be controllable to within a few percent. The ability of this technique to generate smooth focal profiles is demonstrated using a small KrF discharge oscillator-preamplifier system.

20 DISTRIBUTION / AVAILABILITY OF ABSTRACT ☒ UNCLASSIFIED/UNLIMITED ☐ SAME AS RPT ☐ DTIC USERS	21 ABSTRACT SECURITY CLASSIFICATION UNCLASSIFIED
22a NAME OF RESPONSIBLE INDIVIDUAL Robert Lehmberg	22b TELEPHONE (Include Area Code) (202) 767-2730 22c OFFICE SYMBOL Code 4730

DD FORM 1473, 84 MAR 83 APR edition may be used until exhausted
All other editions are obsolete

SECURITY CLASSIFICATION OF THIS PAGE

CONTENTS

USE OF INCOHERENCE TO PRODUCE SMOOTH AND CONTROLLABLE IRRADIATION PROFILES WITH KrF FUSION LASERS

INTRODUCTION

Direct-drive laser fusion requires high intensity laser light that uniformly illuminates a spherical target surface. Theoretical studies have shown [1-3] that acceptable spherical uniformity can be achieved with direct illumination by overlapping a limited number ($\gtrsim 20$) of focused beams, provided that each individual beam profile is smooth and reproducible. Earlier efforts to obtain such profiles, however, had been frustrated by the inherent imperfections in high power multistage lasers. The cumulative effect of small amplitude and phase aberrations introduced by each optical element of a multistage laser is to produce large random aberrations in the output beam. In the usual configuration, where the target is placed in the quasi near-field of the focusing lens, these aberrations tend to produce large random intensity nonuniformities at the target surface.

One possible solution to this problem is a technique called Induced Spatial Incoherence (ISI) [4,5]. In this scheme, spatially incoherent light is created by propagating a laser beam of broad spectral bandwidth $\Delta\nu$ through a pair of echelon structures that impose a different time delay at each step. If the delay increments Δt are chosen somewhat larger than the optical coherence time $t_c = 1/\Delta\nu$, the beam is sliced into an array of mutually-incoherent square beamlets. Each of these will independently focus to the same diffraction profile [the $\mathrm{sinc}^2(x)\ \mathrm{sinc}^2(y)$ function] of width $f\lambda/d$, provided that its initial width d is small in comparison to the transverse scalelength s_a of the incident beam aberration. (Here, f is the focal length of the lens, and λ is the mean optical wavelength.) The transient interference pattern produced by superposition of these beamlets will evolve randomly in times of order t_c. The target will therefore ignore this rapidly shifting structure, and respond only to the time-averaged intensity $\langle I(\vec{x})\rangle \propto \mathrm{sinc}^2(x)\ \mathrm{sinc}^2(y)$ if its hydrodynamic response time t_h satisfies $t_h >> t_c$. For example, an optical bandwidth $\Delta\nu = 30\ \mathrm{cm}^{-1}$ (easily achieved in Nd:glass or KrF lasers) provides $t_c \simeq 1$ psec, whereas t_h is typically ≈ 1 nsec in large high-gain pellet designs.

In its present application, the ISI technique requires the echelons to be placed at the output of the laser. This restriction stems from self-focusing effects in glass lasers, and from the necessity of maintaining spatial coherence in any harmonic conversion crystals. The near-field nonuniformities associated with an array of beamlets would seed self-focusing if one attempted to amplify those beamlets in a

Manuscript approved May 22, 1986.

multistage glass laser, [6] where the nonlinear phase shifts are typically $B > 5$ radians. By placing the echelons at the output, one can control self-focusing, and thus maintain an acceptable degree of transverse beam uniformity over distance $\sim d$. This configuration would require a large number of optically coated echelon steps operating at high optical fluence levels if it were used in a fusion reactor with large apertures and multiple beam lines. For example, a recent conceptual design study for the Sirius-M reactor [7] concluded that in order to use ISI at $\lambda = 1/4$ μm, one would require 240 steps in each transverse direction for each of 32 drive beams. Another issue raised by this ISI configuration is that of efficiency. Approximately 15% of the energy at the focal plane will diffract into sidelobes, and most of that energy would have to be discarded in order to achieve good illumination uniformity.

Although self-focusing remains a serious problem in glass lasers, it is far less important in KrF systems [8-13], where intensities are typically < 10 MW/cm^2, and the amplifying medium is gaseous. A reduction of the nonlinear phase shift to $< 1/2$ radian could eliminate the necessity of placing the echelons at the laser output, thereby opening the way for several possible improvements. For example, instead of the reactor configuration discussed above, one could produce the beamlets by a single pair of echelons at a low power stage, spatially-filter them to eliminate the sidelobes, then optically-relay them through each of the main amplifier chains. As long as these beamlets remain small in comparison to the transverse scalelength of the aberrations (e.g., due to passive optics, turbulence, and nonuniformities in the amplifier excitation), they can focus to the sinc^2 profile without any sidelobes at the target. One issue raised by this scheme is the fact that the spatially-filtered beamlets would have Gaussian-like intensity profiles that remain stationary within the amplifier apertures; hence, there is a possibility that they (and therefore the target beam profile) could be affected by gain saturation.

This paper describes an alternative ISI scheme shown in Fig. 1, in which the echelons are completely eliminated. The concept, which will be referred to as echelon-free ISI, is basically an image projection technique that projects the desired spatial profile onto the target via the laser system, using partially-coherent light. The information required to reproduce this profile is transported through the laser by a multitude of small coherence zones, rather than any large whole-beam structure. Thus, the coherence zones play essentially the same role as the beamlets do in conventional ISI, except that their near-field intensity profiles are not "frozen in" by any echelon steps. A large, spatially-incoherent beam of amplitude $E_0(\bar{x},t)$ is generated by broadband amplified spontaneous emission (ASE) in a mirrorless or spatially multimode laser oscillator. Its central portion illuminates a transparency or variable-density absorber VDA, whose spatial transmission function $F(\bar{x})$ (of effective aperture D_0) is the smoothly-varying irradiation profile required by the target. [2,3] By choosing the oscillator aperture sufficiently large, and placing it close to VDA, one can satisfy the following conditions: (i) The light within D_0 must remain incoherent, with a broad, smooth angular power spectrum $\bar{\gamma}_0(\bar{\theta})$ of width $\Delta\theta >> \lambda/D_0$.

DESIRED IRRADIATION PROFILE F(r) IS IMAGED ONTO THE TARGET THROUGH THE LASER CHAIN, USING PARTIALLY- COHERENT LIGHT

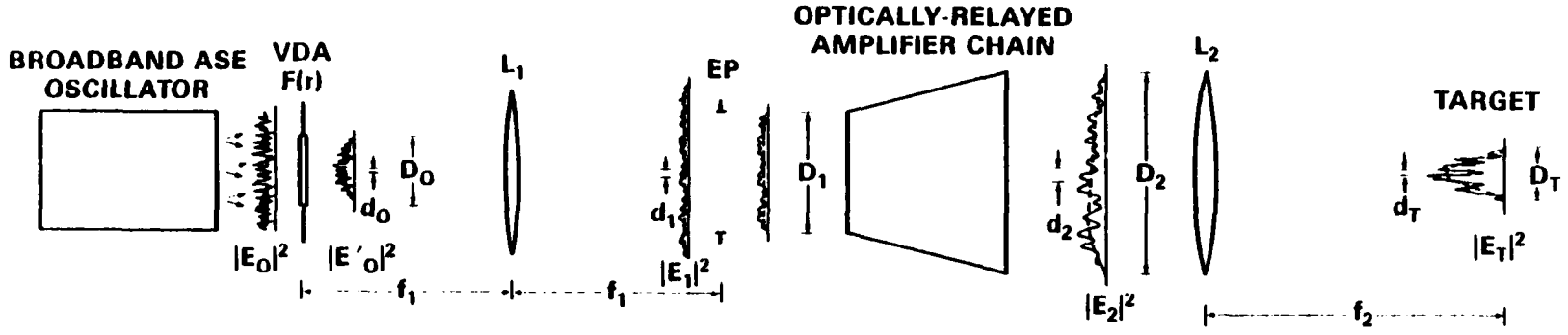

Fig. 1 — Schematic diagram of a spatially-incoherent broadband laser system for smooth, controllable illumination of fusion targets. The solid line profiles show typical instantaneous intensities $|E|^2$, while the dashed lines show the time-averaged intensities $\langle |E|^2 \rangle$.

(ii) To a good approximation, it must be statistically homogeneous; i.e., both $\tilde{\gamma}_0(\bar{\theta})$ and the time-averaged incident intensity $<I_0> = <|E_0(\bar{x})|^2>$ must remain nearly uniform across D_0. Any deviation from condition (ii) is likely to arise from the largest angle modes of $\tilde{\gamma}_0(\bar{\theta})$, which may experience some gain nonuniformity within the ASE oscillator. These modes can be readily eliminated, however, by slightly overfilling the aperture D_1 at the laser-chain entrance pupil EP, as shown in Fig. 1. If conditions (i) and (ii) are satisfied, then the beam $E_0'(\bar{x},t)$ transmitted through VDA can be described by the spatial autocorrelation function

$$\Gamma_0'(\bar{X},\bar{\xi}) \equiv <E_0'(\bar{x})E_0'^*(\bar{x}')> \simeq <I_0>F(\bar{X})\gamma_0(\bar{\xi}). \tag{1}$$

Here, $\bar{X} \equiv \frac{1}{2}(\bar{x} + \bar{x}')$ and $\bar{\xi} \equiv \bar{x} - \bar{x}'$ define, respectively, the mean position and separation of the transverse coordinates, while $\gamma_0(\bar{\xi})$ [which is the Fourier transform of $\tilde{\gamma}_0(\bar{\theta})$] is nonvanishing only within a coherence zone $d_0 \gtrsim \lambda/\Delta\theta << D_0$ (E.g., see Fig. 1). The correction term to the approximation in (1) is of order d_0^2/D_0^2, which is negligible for the ratios $d_0 < D_0/40$ envisioned for actual KrF systems.

Because VDA and EP are located at opposite focal planes of lens L_1, the amplitude $E_1(\bar{x}, t)$ at EP will be the Fourier transform of $E_0'(\bar{x}, t)$. The autocorrelation function $<E_1(\bar{x})\ E_1^*(\bar{x}')>$ at EP then becomes

$$\Gamma_1(\bar{X}, \bar{\xi}) = <I_1(\bar{X})>\ \tilde{F}(\bar{\xi}), \tag{2}$$

where $<I_1(\bar{X})> = <|E_1(\bar{X})|^2> \propto \tilde{\gamma}_0(\bar{X}/f_1)$ is the average intensity, which may vary slowly across D_1, and

$$\tilde{F}(\bar{\xi}) = \int F(\bar{X}') \exp\left(-i\frac{k}{f_1}\bar{X}'\cdot\bar{\xi}\right) d^2X', \qquad \tilde{F}(0) = 1, \tag{3a}$$

$$\to 0 \quad \text{for} \quad |\bar{\xi}| > d_1 \simeq \lambda f_1/D_0 << D_1 \tag{3b}$$

is the Fourier transform of the absorber function, whose coherence width is $d_1 \simeq \lambda f_1/D_0 << D_1$. For example, a Gaussian profile

$$F(\bar{X}) = (1/\pi R_0^2)\exp(-|\bar{X}|^2/R_0^2) \tag{4}$$

of $1/e$ diameter $D_0 = 2R_0$ would transform to $\tilde{F}(\bar{\xi}) = \exp(-|\bar{\xi}|^2/r_1^2)$, with a coherence zone of diameter $d_1 = 2r_1 = (4/\pi)\ \lambda f_1/D_0$. Expressions (3a, b) show clearly that the intensity and phase information needed to reproduce $F(\bar{X})$ is now contained in the small coherence zones of width d_1, rather than any large-scale beam structure of width $\sim D_1$ (Fig. 1).

Beyond EP, the light is relayed through the aberrated multistage amplifier chain to produce an output amplitude $E_2(\bar{x}, t)$ at the focusing lens L_2. (The effects of aberration are illustrated in Fig. 1 by the non-symmetric appearance of the average intensity $<|E_2(\bar{x})|^2>$.) The average intensity $<|E_T(\bar{x})|^2>$ at the target is then given by the general expression

$$<I_T(\bar{x})> = \left|\frac{k}{2\pi f_2}\right|^2 \int d^2X' \int d^2\xi' \, \Gamma_2(\bar{X}', \bar{\xi}') \exp\left[-i\frac{k}{f_2}\bar{x}\cdot\bar{\xi}'\right], \tag{5}$$

where $\Gamma_2(\bar{X}', \bar{\xi}')$ is the autocorrelation function at L_2. In the ideal case, where self-focusing is negligible, the coherence zones at L_2 will convey essentially the same information as those at EP, provided that they remained small in comparison to the local apertures and aberration scalelengths s_a, as they propagated through the laser system. The only change will be the magnification factor $M = D_2/D_1 = d_2/d_1$ due to the expanding apertures. Thus, the output beam will focus to the desired average intensity profile of width $D_T \simeq \lambda f_2/d_2 = D_0 f_2/f_1 M$:

$$<I_T(\bar{x})> = (Mf_1/f_2)^2 <P> F(-Mf_1\bar{x}/f_2), \tag{6}$$

where $<P>$ is the average output power. The transient interference structure (of typical size $d_T = \lambda f_2/D_2 \geq d_0 f_2/f_1 M$) will average out over many coherence times, just as it did in the original ISI technique. In the remainder of this paper, we will examine the perturbing effects of linear and nonlinear aberration, and present preliminary experimental results demonstrating that the technique can produce smooth target beam profiles even under non-ideal conditions.

Because this scheme uses image projection, it bears some resemblance to techniques that use excimer lasers for projection photolithography [14]. The essential difference, however, is that the profile $F(\bar{x})$ lacks the fine structure normally demanded in high resolution lithography; consequently, it does not require large coherence zones that would be susceptible to aberration in the laser system. By contrast, projection photolithography requires considerable care to minimize aberration in the lenses and image projection path.

Echelon-free ISI is compatible with angular multiplexing techniques proposed for excimer fusion drivers [9-13]. For example, a 5 mm coherence zone (appropriate for a 30 cm aperture) would have a 50 μrad diffraction angle at $\lambda = 0.25$ μm, whereas the angular separation of the multiplexed beams would typically be >1 mrad. The beam at EP need not be exactly imaged onto lens L_2; in fact a significant amount of free propagation would be tolerable within the amplifier system. The only requirement is that any spreading of the coherence zones due to diffraction must also remain small in comparison to the apertures and aberration scalelengths. Thus, the technique would not require image relaying at the large-aperture final amplifier, or even in the temporal decoding paths [9-13] that follow it. For example, the diffraction length $z_d \simeq d^2/\lambda$ of a 5 mm coherence zone would be $\sim$100 meters

(300 ns). Image relaying would be required in most of the amplifier chain, including the temporal encoding paths near the input. For the small apertures near the input, however, a separate telescope in each encoding path would be a minor price to pay for controllable high quality beams on target.

ABERRATION EFFECTS

Using a simplified model of multiplexed excimer lasers, we have carried out a detailed perturbation analysis to evaluate the effects of linear aberration, self-focusing, amplifier saturation, and diffraction on the focal profile with echelon-free ISI. This section will outline the assumptions and results of that analysis; a more detailed derivation will be given in a later publication. A perturbation treatment should be appropriate for this problem because the effects due to aberration must remain small if the technique is to be at all useful. In treating the individual aberration mechanisms, the key simplifying assumption is the thin window model, which ignores the effects of diffraction in the locality at which the aberration is created. This can be justified by the fact that most aberration occurs in optical elements short in comparison to the diffraction lengths $z_d = d^2/\lambda$ associated with the coherence zones. (e.g., recall the z_d estimate given above.)

Linear aberration can arise from turbulence and nonuniform excitation, or from passive optical elements such as lenses, mirrors, and apertures. In the thin window approximation, it is described by a nonuniform intensity transmission $T(\vec{x})$ and phase shift $\phi(\vec{x})$, which relate the incident and aberrated amplitudes by the expression $E'(\vec{x},t) = E(\vec{x},t)[T(\vec{x})]^{1/2}\exp[i\phi(\vec{x})]$. The corresponding correlation functions therefore satisfy

$$\Gamma'(\vec{X},\vec{\xi}) = \Gamma(\vec{X},\vec{\xi})\ [T(\vec{x})\ T(\vec{x}')]^{1/2}\ \exp\ [i\phi(\vec{x}) - i\phi(\vec{x}')],$$

where $\vec{x} = \vec{X} + \frac{1}{2}\vec{\xi}$ and $\vec{x}' = \vec{X} - \frac{1}{2}\vec{\xi}$. Because $|\vec{\xi}|$ is limited to coherence zones d small in comparison to the aberration scalelength s_a, one can approximate this expression by a second order expansion in the small quantity $|\vec{\xi}|/s_a \sim d/s_a$; i.e.,

$$\Gamma'(\vec{X},\vec{\xi}) \simeq \Gamma(\vec{X},\vec{\xi})\ T(\vec{X})\ \{1 + i\vec{\xi}\cdot\nabla\phi(\vec{X}) - \frac{1}{2}\vec{\xi}\cdot[\ (\nabla\phi)\ (\nabla\phi) - \frac{1}{4}\nabla\nabla(lnT)\ ]\cdot\vec{\xi}\}, \qquad (7)$$

where $\nabla \equiv \partial/\partial\vec{X}$ operates in the transverse plane.

Self-focusing is a potentially serious limitation because it can affect the beam on scalelengths comparable to the coherence zones. The main problem arises from those contributions, such as the third-order electronic susceptibility, [6] whose nonlinear refractive index n_2 can respond "instantaneously" to

the stochastic intensity fluctuations (i.e., on a time scale $< t_c$). In the thin window model, this contribution will generate an instantaneous nonlinear phase shift $\eta|E(\bar{x},t)|^2$, where $\eta = (8\pi/n_0 c)\frac{1}{2} n_2 k L$, n_0 is the linear refractive index, and L is the thickness of the medium. The transmission through this medium is then described by the relation

$$\Gamma'(\bar{X},\bar{\xi}) = \langle E(\bar{x},t)E^*(\bar{x}',t) \exp[i\eta|E(\bar{x},t)|^2 - i\eta|E(\bar{x}',t)|^2]\rangle,$$

where $(\bar{X},\bar{\xi})$ are related to $(\bar{x},\bar{x}')$ in the usual way. Because the incident light is chaotic, the amplitudes $E(\bar{x},t)$ and $E(\bar{x}',t)$ should satisfy Gaussian statistics; it is therefore permissible to expand the exponential and apply Gaussian factorizations to the resulting amplitude products. Carrying this out to second order, and recalling that $\bar{\xi}$ is a small parameter, one obtains the approximate result

$$\Gamma'(\bar{X},\bar{\xi}) \simeq \Gamma(\bar{X},\bar{\xi})\{1 + 2i\bar{\xi}\cdot\nabla\langle B(\bar{X})\rangle - 2[1 - |\gamma(\bar{X},\bar{\xi})|^2]\langle B(\bar{X})\rangle^2\}, \tag{8}$$

where $\gamma(\bar{X},\bar{\xi}) \equiv \Gamma(\bar{X},\bar{\xi})/\langle I(\bar{X})\rangle$, and

$$\langle B(\bar{X})\rangle \equiv \eta\langle|E(\bar{X})|^2\rangle = \eta\langle I(\bar{X})\rangle \tag{9}$$

is the average nonlinear phase shift, which must be kept as small as possible ($\langle B\rangle^2 << 1$). For fused quartz ($n_0 \simeq 1.5$, $n_2 \simeq 10^{-13}$ esu [6]), Eq. (9) gives $\langle B\rangle \simeq 7\times 10^{-5}\ \langle I(MW/cm^2)\rangle \cdot L(cm)$ at $\lambda = 0.25\mu m$.

The aberrating effects of gain saturation depend upon how rapidly the stochastic intensity fluctuations $I(\bar{x},t) - \langle I(\bar{x})\rangle$ occur within the relaxation time τ of the excimer population. For fluctuation times $\sim t_c << \tau$ in a homogeneously broadened laser medium (e.g., KrF), [9] the large-signal gain $G(\bar{x})$ will respond only to the average intensity $\langle I(\bar{x})\rangle$. The relationship between the incident and amplified correlation functions thus follows from the elementary expression $E'(\bar{x},t) = [G(\bar{x})]^{1/2} E(\bar{x},t)$. Because $G(\bar{x}) = G(\langle I(\bar{x})\rangle)$ varies slowly within the coherence zones, it can be expanded in the same manner as the linear transmission $T(\bar{x})$ treated previously; i.e.,

$$\Gamma'(\bar{X},\bar{\xi}) \simeq \Gamma(\bar{X},\bar{\xi})\ G(\bar{X})\ [\,1 + \frac{1}{8}\bar{\xi}\cdot(\nabla\nabla\ ln\ G)\cdot\bar{\xi}\,]. \tag{10}$$

Using a perturbation treatment of the laser amplifier equations, one can show that the correction term due to intensity fluctuations with nonvanishing values of t_c/τ is approximately

$$\Delta\Gamma'(\bar{X},\bar{\xi}) \simeq -[g_1(\bar{X}) - g_2(\bar{X})\,|\,\gamma(\bar{X},\bar{\xi})\,|^2\,]\,\Gamma'(\bar{X},\bar{\xi})\ t_c/\tau,$$

where $\gamma(\bar{X},\bar{\xi})$ is the reduced correlation function defined previously, and $g_1(\bar{X})$, $g_2(\bar{X})$ are slowly-varying functions satisfying $|g_1| \sim |g_2| \sim 1$. If this term were large, it could be an additional source of small-scale aberration due to $|\gamma(\bar{X},\bar{\xi})|^2$; however, for typical values of $t_c \sim 1$ *ps* ($\Delta\nu = 30\text{cm}^{-1}$) and $\tau \sim 2$ *ns*, it remains negligible.

Eximer Laser Model

The aberration terms can now be incorporated into a simple laser model to provide useful expressions for the target beam perturbation. Aberration due to the amplifier chain alone is modeled by a single thin window W_1 of nonuniform gain $G(\bar{x})$ and phase $\phi_1(\bar{x})$ imaged at or near the entrance pupil EP. Thus, the autocorrelation function $\Gamma'_1(\bar{X},\bar{\xi})$ at the output of the laser chain can be related to the appropriately-scaled input function $\Gamma_1(\bar{X}/M, \bar{\xi}/M)/M^2$ [Eq. (2)] by expression (7), with the replacement $T(\bar{X}) \rightarrow G(\bar{X})$ and $\phi(\bar{X}) \rightarrow \phi_1(\bar{X})$. [In general, the nonuniformity of $G(\bar{X})$ may include the effect of apodization in addition to those of nonuniform excitation and losses within the amplifiers.] The single-window approximation is justified by the fact that most aberration is likely to occur in either the amplifier modules, which are normally imaged onto EP, [11-13] or in optical elements (e.g., telescope lenses) that lie in the quasi near-field of those modules. Self focusing effects are expected to remain negligible within the amplifier chain because of the low intensities required in excimer lasers. For example, at typical KrF output intensities <15 MW/cm^2, [9] expression (9) gives $<B> \; < 10^{-3}$ L(cm) in fused quartz; at these intensity levels, even a total nonlinear pathlength of 50 cm would generate only $<B> \; < 0.05$ radian.

A second thin window W_2, which would be located near lens L_2, models linear and nonlinear aberration in the focusing optics and delay path (required for temporal decoding [9-13]) beyond the amplifier chain. Diffraction in this delay path is modelled by allowing a free propagation distance z_{12} between the windows; the correlation function $\Gamma_2(\bar{X},\bar{\xi})$ for light incident at W_2 can then be related to $\Gamma'_1(\bar{X},\bar{\xi})$ by paraxial diffraction theory [15]:

$$\Gamma_2(\bar{X},\bar{\xi}) = \left(\frac{k}{2\pi z_{12}}\right)^2 \int d^2X' \int d^2\xi' \, \Gamma'_1(\bar{X}',\bar{\xi}') \exp\left[i \frac{k}{z_{12}} (\bar{X}' - \bar{X}) \cdot (\bar{\xi}' - \bar{\xi})\right] \qquad (11)$$

In the spirit of the perturbation treatment, this integral is evaluated only up to second order in the small quantity d_{12}/s_a, where $d_{12} \equiv \lambda \, z_{12}/d_2$ represents the diffractive blurring of a coherence zone of initial width $d_2 = Md_1$. The focusing optics and delay paths are more likely to introduce phase aberration $\phi_2(\bar{x})$ (e.g., due to thermal gradients), rather than any significant transmission nonuniformity; hence, the transmission $T \lesssim 1$ will be treated as uniform in W_2. Combining this consideration with the nonlinear perturbation terms derived previously, one obtains at the output of W_2,

$$\Gamma'_2(\bar{X},\bar{\xi}) \simeq \Gamma_2(\bar{X},\bar{\xi})\ T\left\{1 + i\,\bar{\xi}\cdot\nabla\phi_2\,(\bar{X}) - \frac{1}{2}\,\bar{\xi}\cdot(\nabla\phi_2)\,(\nabla\phi_2)\cdot\bar{\xi}\right.$$

$$\left. + 2i\bar{\xi}\cdot\nabla < B(\bar{X}) > - 2\,[1 - |\gamma_2(\bar{X},\bar{\xi})|^2]\, < B(\bar{X}) >^2\right\}, \tag{12}$$

where $\gamma_2(\bar{X},\bar{\xi}) = \Gamma_2\,(\bar{X},\bar{\xi})/< I_2(\bar{X}) >$, and $< B(\bar{X}) >$ is given by Eq. (9) with $< I(\bar{X}) > \rightarrow < I_2(\bar{X}) >$. The average target beam intensity $< I_T(\bar{x}) >$ can then be evaluated by substituting $\Gamma'_2(\bar{X},\bar{\xi})$ into Eq. (5).

Combining the above considerations, and retaining terms only up to second order in the small quantities d_2/s_a, d_{12}/s_a and $<B>$, one can finally evaluate the perturbed target beam profile $< I_T\,(\bar{x}) >$ from Eq. (5). In terms of the average output power

$$< P > = \int T\ G(\bar{X}')\ \frac{< I_1(\bar{X}'/M) >}{M^2} d^2X' \tag{13}$$

and the weighted transverse spatial average

$$\{Q\}_{AV} \equiv \frac{1}{< P >} \int T\ G(\bar{X}')\ \frac{< I_1\,(\bar{X}'/M) >}{M^2} Q(\bar{X}')\ d^2X', \tag{14}$$

which is defined for any well-behaved quantity $Q(\bar{X}')$, one obtains

$$< I_T\,(\bar{x}) > = < I_T^{(0)}\,(\bar{x}) > + < I_T^{(1)}\,(\bar{x}) > + < I_T^{(2)}\,(\bar{x}) > + < I_T^{(NL)}\,(\bar{x}) > , \tag{15}$$

where

$$< I_T^{(0)}\,(\bar{x}) > \equiv (Mf_1/f_2)^2 < P > F\,(-\,Mf_1\,\bar{x}/f_2), \tag{16a}$$

$$< I_T^{(1)}\,(\bar{x}) > \equiv -(f_2/k)\,\{\nabla'\phi\}_{AV}\cdot\nabla\,< I_T^{(0)}(\bar{x}) >. \tag{16b}$$

$$< I_T^{(2)}\,(\bar{x}) > \equiv \frac{1}{2}\,(f_2/k)^2\,\{(\nabla_\mu'\phi)\ (\nabla_\nu'\phi)$$

$$- \frac{1}{4}\nabla_\mu'\nabla_\nu'\,ln\,(TG)\,\}_{AV}\,\nabla_\mu\,\nabla_\nu\,< I_T^{(0)}\,(\bar{x}) >$$

$$- (z_{12}/k)\,\{\nabla_\mu'\nabla_\nu'\phi_2\,\}_{AV}\,\nabla_\mu\,[x_\nu\,< I_T^{(0)}\,(\bar{x}) >], \tag{16c}$$

$$< I_T^{(NL)} (\bar{x}) > \equiv - 2(f_2/k) \{ \nabla' < B > \}_{AV} \cdot \nabla < I_T^{(0)} (\bar{x}) >$$

$$- 2\{ < B >^2 \}_{AV} [< I_T^{(0)} (\bar{x}) > - (Mf_1/f_2)^2 < P > H(\bar{x})], \tag{16d}$$

$$H(\bar{x}) \equiv (\frac{k}{2\pi f_1})^2 \int | \tilde{F} (\bar{\xi}) |^2 \tilde{F} (\bar{\xi}) \exp (-i\frac{k}{f_2} M\bar{x} \cdot \bar{\xi}) \, d^2\xi, \tag{16e}$$

and $\phi(\bar{X}') \equiv \phi_1 (\bar{X}') + \phi_2 (\bar{X}')$ is the total linear phase aberration. [In Eq. (16c), the repeated indices μ, ν imply a summation over the two transverse dimensions.] The zeroth order term (16a) is identical to Eq. (6). Expressions (16b) and (16c) are, respectively, the first and second order perturbations due to linear aberration, and (16d), which is entirely in second order, describes nonlinear effects. In (16d), the first term accounts for beam steering due to a combination of nonlinear refraction and nonuniform intensity, while the $< B >^2$ term describes self focusing in the vicinity of L_2, which results in profile broadening at the target.

The small expansion parameters may be seen more clearly in these expressions by noting that the operators $\nabla' \equiv \partial/\partial\bar{X}'$ and $\nabla \equiv \partial/\partial\bar{x}$ can introduce factors of order $1/s_a$ and $1/D_T$, respectively, where $D_T = D_0 f_2/f_1 M$ is the target beam diameter. Recalling the relationship $D_T = \lambda f_2/d_2$ between D_T and the coherence zone diameter d_2, one can see, for example, that expression (16c) will contain the factors d_2^2/s_a^2 and $d_2 d_{12}/s_a^2$, while (16d) contains the factors $< B > d_2/s_a$ and $< B >^2$. Contributions of order d_{12}^2/s_a^2 and $< B > d_{12}/s_a$ vanish under the conditions assumed here.

It is instructive to relate the linear aberration coefficients to the angular divergence and focal spot parameters that the laser would produce (in the absence of nonlinear aberration) with a plane wave source at EP. In the geometrical optics limit, this relationship can be seen immediately by noting that $\bar{\theta}(\bar{X}') \equiv (1/k) \nabla' \phi(\bar{X}')$ is the refraction angle that an incident axial ray would acquire as it propagates through the aberrated system. The centroid of the aberrated (but spatially coherent) focal distribution would then be given by the intensity-weighted average

$$\{\bar{x}_c\}_{AV} \equiv f_2\{\bar{\theta}\}_{AV} = (f_2/k)\{\nabla' \phi(\bar{X}')\}_{AV}, \tag{17}$$

which is the coefficient in $< I_T^{(1)}(\bar{x}) >$. If the laser could be precisely aligned onto the target, then $\{\bar{x}_c\}_{AV}$ would vanish identically; in practice, however, the random angular "jitter" $\delta\bar{\theta}(\bar{X}')$ due to microturbulence $\delta\phi(\bar{x}')$ in the amplifiers and propagation paths will quickly lead to a small residual misalignment $\{\bar{x}_c\}_{AV} \rightarrow f_2\{\delta\bar{\theta}\}_{AV}$ (Gradual misalignment due to large-scale thermal gradients would presumably be corrected by an automatic alignment system.) For the second moment $\{\bar{x}_c \, \bar{x}_c\}_{AV}$, geometrical optics would give $f_2^2\{\bar{\theta}\,\bar{\theta}\}_{AV}$; however, a more complete treatment including diffraction yields the result

$$\{\bar{x}_c\ \bar{x}_c\}_{AV} = (f_2/k)^2\{\ (\nabla'\phi)\ (\nabla'\phi) - \frac{1}{4}\nabla'\nabla'\ ln\ (TG)\ \}_{AV}, \tag{18}$$

which accounts for the first two terms of $<I_T^{(2)}(\bar{x})>$. The final term in $<I_T^{(2)}\ (\bar{x})>$ (which is the only one that involves the free propagation path) has the coefficient $(z_{12}/k)\ \{\nabla'\nabla'\phi_2\}_{AV}$, and arises from the combined effects of diffraction and phase aberration beyond the laser chain. This expression represents a phase curvature, so most of it can be compensated by a small axial adjustment and/or tilting of the focusing lens, thus leaving only a residual contribution due to the angular jitter $\delta\bar{\theta}_2$. Substituting these results into Eqs. (16b,c) one finally obtains

$$<I_T^{(1)}\ (\bar{x})> = -\{\bar{x}_c\}_{AV} \cdot \nabla\ <I_T^{(0)}\ (\bar{x})>, \tag{19a}$$

$$<I_T^{(2)}(\bar{x})> = \frac{1}{2}\{x_{c\mu}\ x_{c\nu}\}_{AV}\ \nabla_\mu\ \nabla_\nu\ <I_T^{(0)}\ (\bar{x})>$$

$$- z_{12}\{\nabla_\mu'\theta_{2\nu}\}_{AV}\ \nabla_\mu \left[x_\nu\ <I_T^{(0)}\ (\bar{x})>\right]. \tag{19b}$$

One can obtain expressions for the relative magnitudes of the various perturbation terms by choosing for $F(\bar{x})$ the Gaussian profile defined in Eq. (4). This yields the desired target beam

$$<I_T^{(0)}\ (\bar{x})> \rightarrow (<P>/\pi R_T^2)\exp\ (-|\ \bar{x}\ |^2/R_T^2), \tag{20}$$

where $R_T = D_T/2 = R_0\ f_2/f_1 M$, and the relative perturbation terms:

$$<I_T^{(1)}\ (\bar{x})>/<I_T^{(0)}\ (\bar{x})> \rightarrow 2\ (\{\bar{x}_c\}_{AV}/R_T) \cdot \bar{x}/R_T, \tag{21a}$$

$$<I_T^{(2)}\ (\bar{x})>/\ <I_T^{(0)}\ (\bar{x})> \rightarrow -\left[\{x_{c\mu}x_{c\nu}\}_{AV}/R_T^2 + z_{12}\{\nabla_\mu'\theta_{2\nu}\}_{AV}\right](\delta_{\nu\mu} - 2x_\mu x_\nu/R_T^2), \tag{21b}$$

$$<I_T^{(NL)}\ (\bar{x})>/\ <I_T^{(0)}\ (\bar{x})> \rightarrow -2\{\ <B>^2\ \}_{AV}\left[1 - \frac{1}{3}\exp\ (2\ |\bar{x}|^2/3R_T^2)\right]$$

$$+ d_2\ \{\nabla'<B>\}_{AV} \cdot \bar{x}/R_T, \tag{21c}$$

where $d_2 = 4f_2/kR_T$.

Numerical Estimates

If the alignment and focusing systems are optimized to eliminate the average (non-jitter) components of $\{\bar{x}_c\}_{AV}$ and $\{\nabla' \bar{\theta}_2\}_{AV}$, then the linear perturbations will normally be dominated by the phase aberration terms $f_2^2 \{\theta_\mu \theta_\nu\}$ in $\{x_{c\mu} x_{c\nu}\}_{AV}$. The diagonal elements of this matrix, which predominate under random phase conditions, are positive and will tend to broaden $< I_T (\bar{x}) >$. Their contribution to expression (21b), of magnitude

$$Q_0 \equiv \{|\bar{x}_c|^2\}_{AV}/R_T^2 \simeq f_2^2 \, \theta_{RMS}^2 / R_T^2 \tag{22}$$

(where $\theta_{RMS} \equiv \{|\bar{\theta}|^2\}_{AV}^{1/2}$) indicates that this perturbation will be $< 10\%$ if R_T is chosen $\geq 3 f_2 \theta_{RMS}$. The magnitudes of the residual terms in expressions (21a,b) can be estimated by noting that the angular jitter $\delta\bar{\theta}(\bar{X}')$, of RMS value $\delta\theta_{RMS}$ and transverse scalelength s_J, will have $N_J \simeq D_2^2/s_J^2$ independent contributions within aperture D_2. One then obtains

$$Q_1 \equiv |\{\bar{x}_c\}_{AV}|/R_T \rightarrow f_2 \, \delta\theta_{RMS}/R_T \, N_J^{1/2} \simeq s_J \, f_2 \delta\theta_{RMS}/D_2 \, R_T$$

$$Q_2 \equiv z_{12} |\{\nabla' \bar{\theta}_2\}_{AV}| \rightarrow z_{12} \delta\theta_{RMS}/s_J \, N_J^{1/2} \simeq z_{12} \, \delta\theta_{RMS}/D_2,$$

or in comparison to Q_0,

$$Q_1/Q_0 \simeq (s_J/D_2) \;\; (R_T/f_2 \, \theta_{RMS}) \;\; (\delta\theta_{RMS}/\theta_{RMS}) \tag{23a}$$

$$Q_2/Q_0 \simeq (z_{12}/f_2) \;\; (R_T/D_2) \;\; (R_T/f_2 \, \theta_{RMS}) \;\; (\delta\theta_{RMS}/\theta_{RMS}) \tag{23b}$$

For typical cases, where $R_T/f_2\theta_{RMS} \sim 3$–$5$ (corresponding to $Q_0 \sim 0.1$–0.04), $R_T/D_2 \sim 0.01$, $s_J/D_2 < 0.05$, and $z_{12}/f < 5$, the ratios (23a,b) remain small if $\delta\theta_{RMS} < \theta_{RMS}$. The small magnitude of (23b) confirms the earlier statement that the free propagation path will have little effect as long as the coherence zones remain small in comparison to aberration scalelengths.

The nonlinear perturbations will normally be dominated by the $2\{< B >^2\}_{AV}$ term of expression (21c). The largest contributions to $< B >$ are likely to be generated by optical elements such as focusing lenses or windows located in the high intensity decoded beams beyond the final amplifier stage. For example, a 0.25 μm beam of intensity 400 MW/cm^2 (e.g., 2 J/cm^2 in a 5 ns pulse) will, according to expression (9), produce $< B > \simeq 0.15$ radian in 5 cm of fused quartz. Allowing for an additional contribution of 0.05 radian from the amplifiers, one finds $< B > \simeq 0.20$ radian, and thus

$2\{<B>^2\}_{AV} \simeq 8\%$. The ambient atmosphere within the long (50-100 m) decoding paths may also produce a significant contribution to $<B>$, unless some care is taken to minimize its nonlinear refractive index. One possibility, which would also eliminate any rotational SRS, [16] would be to overfill these paths with one of the lighter inert gases. For example, a calculation of the third order nonlinear susceptibility [17] of Ne at 0.25 μm (using tabulated oscillator strengths [18]) gives $n_2/N \simeq 10^{-37}$ esu; hence, Eq. (9) yields $<B> \simeq 2.8 \times 10^{-7}$ p (Amagats) I (MW/cm^2) L (m), where p is the pressure. Assuming 400 MW/cm^2 in a 100 meter path at atmospheric pressure, one obtains $<B> \simeq 0.01$ radian. The n_2/N of most other gases with lower-lying energy levels (including the heavier inert gases, such as Xe [17]) can exceed this value by at least an order of magnitude.

The nonlinear beam steering term $d_2\{\nabla_\perp <B>\}_{AV}$ can arise from either a large-scale asymmetry in the beam, or a number of small random intensity nonuniformities. In either case, its magnitude will be approximately $d_2\delta<B>_{RMS}/D_2$, where $\delta <B>_{RMS}$ is the RMS nonuniformity of $<B>$. In comparison to the $2\{<B>^2\}_{AV}$ term, one obtains

$$d_2|\{\nabla_\perp <B>\}_{AV}|/2\{<B>^2\}_{AV} \approx (d_2/2D_2)\,\delta<B>_{RMS}/\{<B>^2\}_{AV}, \tag{24}$$

which remains small in a typical case, such as $\{<B>\}_{AV} \simeq 0.2$ and $d_2/D_2 < 0.03$.

The theory shows that the total intensity perturbation due to both linear and nonlinear aberrations can readily be reduced below 20%. Moreover, this perturbation is to a large extent controllable. The spatial averaging process embodied in coefficients such as $\{\bar{x}_c\,\bar{x}_c\}_{AV}$ and $\{<B>^2\}_{AV}$ tends to reduce large uncontrollable shot-to-shot variations, while the $\bar{x}$—dependent functions in $<I_T^{(2)}(\bar{x})>$ and $<I_T^{(NL)}(\bar{x})>$, which are smooth and well-defined, tend only to broaden the profile somewhat. If the coefficients can be controlled to within 10%, then the net random perturbation would be reduced to $<2\%$.

EXPERIMENT

A demonstration of the above technique for generation of smooth output beam profiles was performed with a small KrF laser system. Figure 2 shows the experimental setup. The oscillator and amplifier are U.V. pre-ionized discharge lasers similar to the ones described in reference (8), with gain volumes of $0.3 \times 2 \times 30$ cm^3 and $1 \times 5 \times 100$ cm^3, respectively. Nominal pulse duration of the gain is 20 ns. The oscillator was operated within a low-Q resonant cavity formed by the high reflectivity flat mirror M_1 and an uncoated fused silica flat M_2 serving as output mirror. Because no frequency-selective elements are present within the cavity, the oscillator bandwidth is expected to ~ 50 cm^{-1} [8].

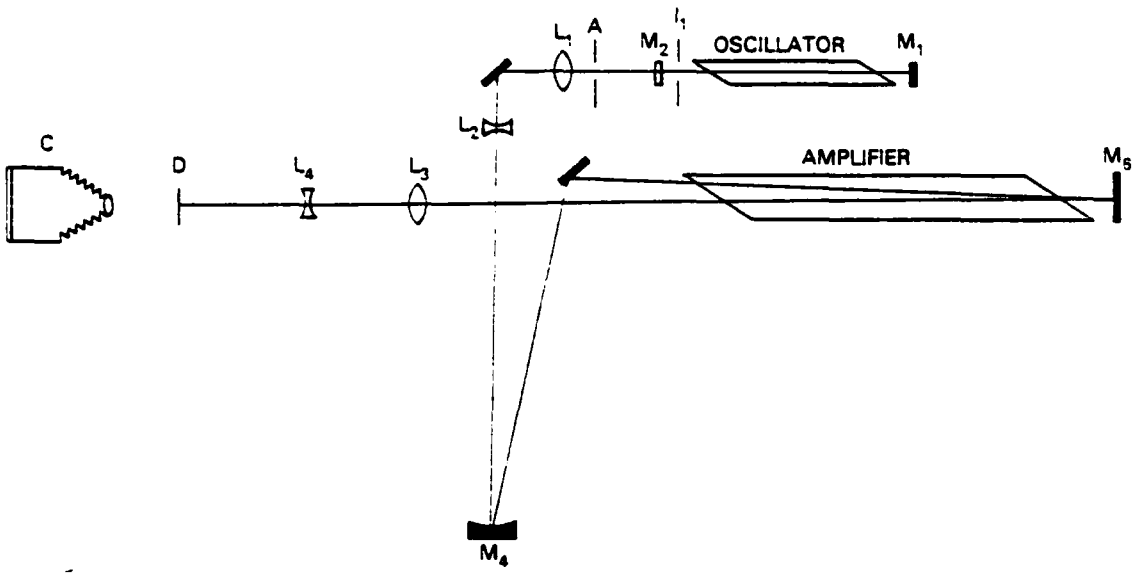

Fig. 2 — Experimental setup of the broadband KrF oscillator-preamplifier system. The degree of spatial incoherence at aperture A is controlled by the iris I_1.

The oscillator could be operated to provide either a spatially-coherent or an incoherent beam by adjusting the aperture of iris I_1. For coherent operation, I_1 was reduced to $\sim$1 mm, giving an observed output beam divergence close to diffraction-limited. With I_1, fully opened, the oscillator operated in a spatially-incoherent, highly-multimode regime with a measured beam divergence $\sim 2 \times 6$ mrad^2.

Output from the oscillator illuminates a circular aperture A, which plays the role of VDA in Fig. 1. The optical elements L_1,L_2 and M_4 project the light at A into its far-field and expand the image. They are equivalent to the L_1 of Fig. 1. The beam is then amplified in two passes through the amplifier. The size and shape of the beam in the amplifier depend upon the operating mode of the oscillator. In the coherent regime, the beam at the amplifier input looks like an Airy pattern with diameter $\sim$2 mm. In the incoherent regime, the beam has dimensions of 0.5×2 cm^2.

Lenses L_3 and L_4 project the Fourier-transform of the amplifier output beam to a diffuser D, which is equivalent to the target plane of Fig. 1. The image of the beam at the diffuser is photographed from behind by a simple open shutter camera. Spatial resolution of this setup is $\sim$0.1 mm. This technique is a good way to attenuate the intense laser beam, and was extensively tested [19]. Polaroid type 55 film was used in these preliminary experiments.

Figure 3 shows the beam profiles obtained in the two regimes. The coherent beam (Fig. 3a) collected information from all the aberrations, partial obscurations, amplifier gain striations, and distortions of the optical system. The incoherent beam (Fig. 3b) shows dramatic improvement in its smooth output profile. In addition to achieving a more uniform illumination of the aperture, one can readily remove most of the distortions observed with the coherent beam from this small laser system by better alignment and higher quality (and undamaged) optical components. However, these problems are

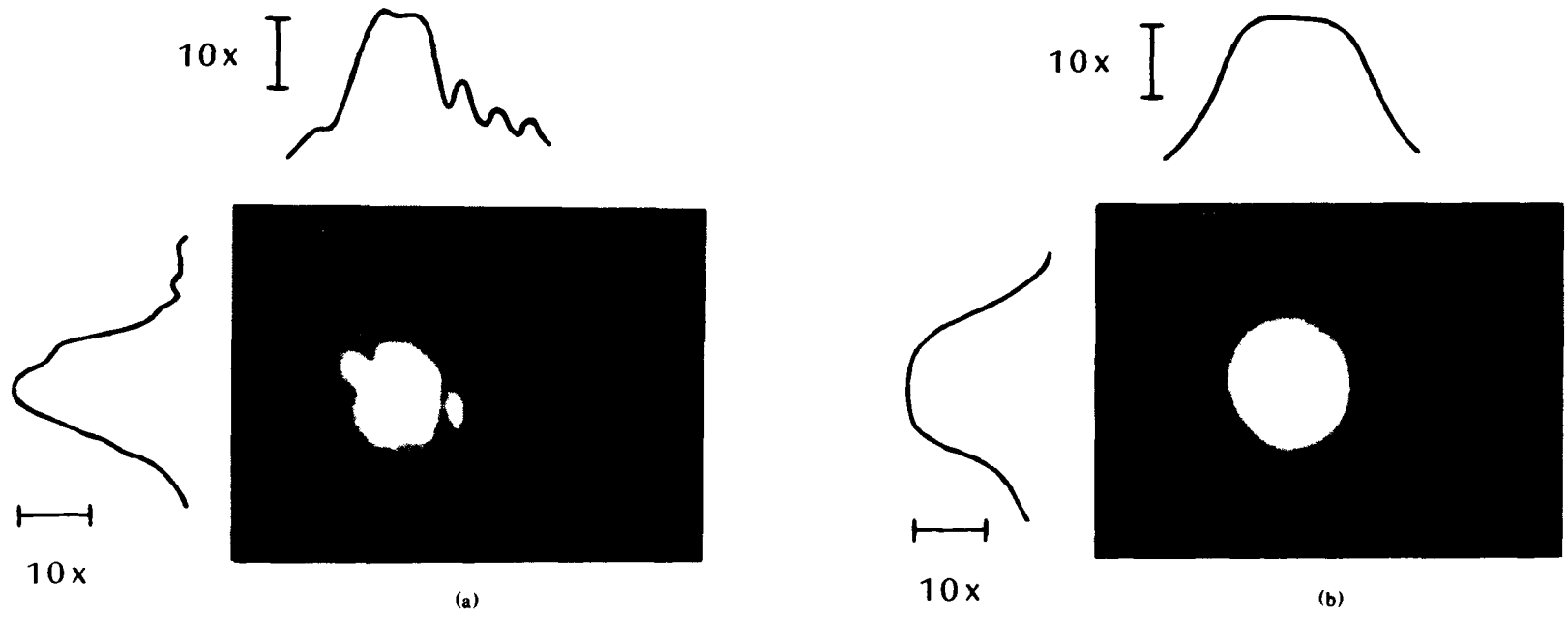

Fig. 3 — Beam profiles observed at the diffuser D, which is located at the image plane of aperture A, for (a) spatially-coherent, and (b) incoherent illumination. The densitometer traces show logarithmic intensity profiles across the horizontal and vertical centerlines of the beams.

much more difficult to correct on a large-scale laser system, and there the echelon-free ISI will offer a significant improvement.

The output power level was ~ 1 MW/cm^2; thus, the amplifier was already operating in the saturating regime. When an earlier version of the experiment was performed with the image of aperture A projected directly into the amplifier, the saturation caused strong beam distortion in a bright ring near the edge of the beam. This shows that the amplification of the beam in the far field, as described in this paper, is an essential requirement for generation of a smooth spot on the target.

Without any aberrations in the optical train, one would expect Fig. 3 to show a perfectly relayed image of aperture A. The aberrations result in a distorted image in the case of a coherent beam. For the incoherent beam, however, the aberrations cause only a blurring of the sharp edges, in agreement with the theory.

SUMMARY AND DISCUSSION

Echelon-free ISI appears to be a promising technique for using excimer lasers to generate the smooth and controllable target beam profiles required for direct-drive fusion. In this scheme, the intensity and phase information needed to produce the time-averaged profile $< I_T(\bar{x}) >$ must be transported through the laser system by coherence zones small in comparison to the apertures and linear aberration scalelengths. (In other words, the angular power spectrum of the partially-coherent light must remain broad in comparison to the angular perturbations introduced by the aberration.) Under conditions applicable to KrF, this criterion should ensure that $< I_T(\bar{x}) >$ remains relatively insensitive to both linear aberration and amplifier saturation within the entire laser system. Both theory and experiment have shown that the aberration will tend to broaden and smooth $< I_T(\bar{x}) >$, but will not introduce any small-scale structure. The theory also shows that the broadening is to a large extent controllable because it depends only upon spatial averages of the aberrated quantities over the whole laser aperture. The estimates presented here have indicated that it should be possible to control the functional form of $< I(\bar{x}) >$ to within a few percent, even with a large angularly-multiplexed system. In excimer lasers, where self-focusing is weak (e.g., $< B > < 1/2$ radian), both this and the other modified ISI scheme (suggested in the fourth paragraph of the introduction) offer another important advantage over conventional ISI with the echelons at the output. They not only avoid the problems mentioned in the introduction, but also allow techniques that could change the size and shape of $< I_T(\bar{x}) >$ during the pulse in order to match an imploding pellet.

ACKNOWLEDGMENTS

The authors gratefully acknowledge valuable discussions with Dr. S. P. Obenschain, Dr. S. E. Bodner and Dr. J. Reintjes. In addition, they would like to thank Mr. L. Myers, Mr. Krishnan and Ms. Feng for their help with construction of the laser.

REFERENCES

1. J.E. Howard, "Uniform Illumination of Spherical Laser Fusion Targets," Appl. Opt. **16**, 2764 (1977).

2. S. Skupsky and K. Lee, "Uniformity of Energy Deposition for Laser Driven Fusion," J. Appl. Phys. **54**, 3662 (1983).

3. A.J. Schmitt, "Absolutely Uniform Illumination of Laser Fusion Pellets," Appl. Phys. Lett. **44**, 399 (1984).

4. R.H. Lehmberg and S.P. Obenschain, "Use of Induced Spatial Incoherence for Uniform Illumination of Laser Fusion Targets," Opt. Commun. **46**, 27 (1983).

5. S.P. Obenschain, J. Grun, M.J. Herbst, K. Kearney, C.K. Manka, E.A. McLean, A. Mostovych, J.A. Stamper, R.R. Whitlock, J. Gardner, and R.H. Lehmberg, "Laser-Target Interaction with Induced Spatial Incoherence," Phys. Rev. Lett. **56**, 2807 (1986).

6. D.C. Brown, "High-Peak-Power Nd:Glass Laser Systems" (Springer-Verlag, 1981), Sec. 1.6

7. A.J. Schmitt, R.H. Lehmberg, J.A. Gardner, and S.E. Bodner, in "SIRIUS-M: A Symmetric Illumination, Inertially-Confined Direct-Drive Materials Test Facility," Fusion Technology Institute, University of Wisconsin UWFDM-651 (September 1985), Sec. IV.2.

8. J. Goldhar, W.R. Rapoport and J.R. Murray, "An Injection-Locked Unstable Resonator Rare-Gas Halide Discharge Laser of Narrow Linewidth and High Spatial Quality," IEEE J. Quantum Electron. **QE-16**, 235 (1980); J. Murray, J. Goldhar, and A. Szoke, Laser Program Annual Report-1977, Lawrence Livermore National Laboratory, UCRL-50021-77 (1978), Sec. 7.6.4.

9. D. Eimerl, J. Goldhar, R.R. Jacobs, J.R. Murray, W.R. Rapoport, L.G. Schlitt, and J.C. Swingle," RAPIER Experimental Program," Laser Program Annual Report-1979 Lawrence Livermore National Laboratory, UCRL-50021-79 (1980) p. 7-21 to 7-40; J. Goldhar and L.G. Schlitt, "RAPIER Experiments," Laser Program Annual Report-1981 Lawrence Livermore National Laboratory, UCRL-50021-81 (1982) p. 7-82 to 7-94.

10. F. O'Neill, "High Power KrF Laser Development," Annual Report to the Laser Facility Committee-1984 (Rutherford Appleton Laboratory, Chilton, Didcot, Oxon, UK), RAL-84-049 (1984) Sec. C.

11. A.M. Hunter II, R.O. Hunter, Jr., and T.H. Johnson, "Scaling of KrF Lasers for Inertial Confinement Fusion," IEEE J. Quantum Electron. **QE-22**, 386 (1986).

12. L.A. Rosocha, P.S. Bowling, M.D. Burrows, M. Kang, J. Hanlon, J. McLeod, and G.W. York, Jr., "An overview of Aurora: A Multi-Kilojoule KrF Laser System for Inertial Confinement Fusion," Laser and Particle Beams **4**, 55 (1986).

13. R.H. Lehmberg, S.P. Obenschain, and A.J. Schmitt, "Baseline Design of a 5-7 kJ KrF Laser Facility for Direct Illumination ICF Experiments," Naval Research Laboratory Memorandum Report 5713 (December 31, 1985).

14. K. Jain and R.T. Kerth, "Excimer Laser Projection Lithography," Appl. Opt. **23**, 684 (1984).

15. M. Born and E. Wolf, "Principles of Optics" (Pergamon Press, 1964), Chapt. 10.

16. V.S. Averbakh, A.I. Makarov, and V.I. Talanov, "Simulated Raman Scattering on Rotational and Vibrational Transitions in Nitrogen Gas," Sov. J. Quantum Electron. **8**, 472 (1978).

17. J.F. Reintjes, "Nonlinear Optical Parametric Processes in Liquids and Gases" (Academic Press, 1984), Sec. 4.2.

18. W.L. Wiese, M.W. Smith, and B.M. Glenon, "Atomic Transition Probabilities," National Standard Reference Data Series NSRDS-NBS 4 Vol. 1 (1966).

19. J. Goldhar and J.R. Murray, "An Efficient Double-Pass Raman Amplifier with Pump Intensity Averaging in a Light Guide," IEEE J. Quantum Electron. **QE-20**, 772 (1984).

END

11-86

DTIC